Endocrine, *vol. 18, no. 3, 285–293, August 2002* 0969–711X/02/18:285–293/$20.00

Structural Aspects of Luteinizing Hormone Receptor

Information from Molecular Modeling and Mutagenesis

Francesca Fanelli[1] and David Puett[2]

[1]Delbecco Telethon Institute (DTI) and Department of Chemistry, University of Modena and Reggio Emilia, via Campi 183, 41100, Modena, Italy; and [2]Department of Biochemistry and Molecular Biology, University of Georgia, Athens, GA

The luteinizing hormone receptor (LHR) is a member of the superfamily of G protein–coupled receptors and, in humans, binds two closely related ligands, members of the heterodimeric glycoprotein hormone family. This receptor is an essential component of the reproductive axis in males and females, and a number of naturally occurring pathophysiologic activating and inactivating mutations have been described. This review deals with the current state of knowledge of the structure of LHR based on molecular modeling and the supporting experimental data from engineered and naturally occurring mutations.

Key Words: Lutropin receptor; G protein–coupled receptor; molecular modeling; mutagenesis; luteinizing hormone receptor.

Introduction

The human glycoprotein hormone receptors are members of the G protein–coupled receptor (GPCR) superfamily *(1–5)*. They bind and mediate the actions of four ligands, each of which is a heterodimer comprising an α-subunit that is common to the glycoprotein hormones and a hormone-specific β-subunit *(6)*. Pituitary-derived luteinizing hormone (LH) and placenta-derived chorionic gonadotropin (CG) bind to the LH receptor (LHR), while pituitary-derived follicle-stimulating hormone (FSH) and thyroid-stimulating hormone (TSH) are cognate ligands for the receptors FSHR and TSHR, respectively. LHR, FSHR, and TSHR are homologous proteins containing a relatively large N-terminal ectodomain responsible for high-affinity ligand binding, in addition to the standard characteristics of GPCRs, notably seven transmembrane helices, three extracellular loops, three intracellular loops, and a short C-terminal tail.

Received July 9, 2002; Revised July 18, 2002; Accepted July 18, 2002.

Author to whom all correspondence and reprint requests should be addressed: Dr. David Puett, Department of Biochemistry & Molecular Biology, Life Sciences Building, 120 Green Street, University of Georgia, Athens, GA. E-mail: puett@bmb.uga.edu

LHR is an essential component of the reproductive axis, and its gene, approx 70 kbp in length and located on chromosome 2p21, contains 11 exons and 10 introns *(2,4,5,7,8)*. The first 10 exons encode the majority of the ectodomain, and most of these encode imperfect leucine-rich repeats (LRRs); exon 11 encodes a portion of the ectodomain, the endodomain, and the C-terminal tail *(5,7,8)*.

The only crystal structure of a GPCR is that of bovine rhodopsin *(9)*. Consequently, the available molecular models of the LHR endodomain have been based on ab initio approaches *(10,11)* and, more recently, comparative modeling *(5,12,13)*. The limited information on the ectodomain is derived primarily from comparative modeling with ribonuclease inhibitor *(14–19)*, an LRR protein *(20)*.

This article deals with the current state of knowledge of the LHR structure based on molecular modeling and the supporting experimental data from engineered and naturally occurring mutations.

Molecular Modeling of LHR and Relevant Experimental Results

Comparative Modeling of Ectodomain Based on LRRs

Analysis of the LHR cDNA and genomic structures revealed that the region of the ectodomain encoded by exons 2–8 contains imperfect LRRs of approx 25 amino acid residues, generally corresponding to one repeat per exon *(7,8, 21,22)*. Exon 9, the longest of the first 10 exons, encodes a tandem repeat of LRRs, and Cys-rich clusters are encoded by exons 1 and 10 and portions of exons 9 and 11. One such putative LRR, corresponding to residues 29–52 of hLHR *(19)*, is as follows: LTRLSLAYLPVKVIPSQAFRGLNE.

Several groups have utilized the LRRs in the ectodomain to perform comparative modeling with porcine ribonuclease inhibitor *(14–19)*. The resulting structures have the typical cusped or horseshoe shape characteristic of LRR proteins and differ from one another based on the number of amino acid residues chosen per repeat and, of course, the number of repeats, most of which were either eight or nine in the LHR ectodomain. LRR structures consist of alternating α-helices and β-strands such that the helices form the outer surface and the β-strands define an inner lining of a horseshoe or partial donut structure with the helices and β-strands parallel to each other *(20)*. One such structure is shown in

Fig. 1 for the LHR ectodomain modeled with nine LRRs in the ectodomain *(17)*. Ribonuclease binds to the inner lining of the ribonuclease inhibitor at multiple contact sites *(20)*, and it is tempting to consider that LHR binds its cognate ligands similarly. The most common motif of the inner cusp, β-strands, in LRR proteins is that of an (L/I)-X-(L/I) sequence (cf. positions four to six, i.e. LSL, in the sequence given in the previous paragraph), which is well conserved in LHR, FSHR, and TSHR *(19)*.

Mutagenesis of Ectodomain for Structure-Function Studies and Validation of Homology Models

A number of engineered replacements have been made in the ectodomain of human and rat LHR for structure-function studies *(17,19,23–29)*, often to test the hypothesis that the inner circumference of the purported LRR structure is important in ligand binding *(14–19)*. The experimental approach has been to prepare LHR mutant cDNAs and express the wild-type (WT) and mutant receptors in transiently or stably transfected cells, followed by specific binding of [^{125}I]hCG with intact or solubilized cells. The results of these investigations from several laboratories are summarized in Table 1.

Table 1
Relative Binding Affinities
of Single LHR Ectodomain Mutants (29–220)[a]

LRR1	(K_d^r)	LRR2	(K_d^r)
L		V→A(20)	0.5
^{30}T(A)		I(V)→A(20)	0.5
R→K, D(24)	1.1, 1.7	K→A(20), R,D(24)	0.2, 3.4, 4.3
L→A(20)	—[b]	I→A(20)	—[b]
S		E→A(20), K(25)	0.4, 1.0
L→A(20)	0.9	I→A(20)	—[b]
A(T)		S→A(20)	0.2
Y		^{60}Q→A(20)	0.7
L		I(S)→A(20)	0.3
P		D→A(20)	0.2
V		S→A(20)	—[b]
^{40}K→R, D(18)	2.8, —[b]	L→A(20)	—[b]
V→A(20)	0.3	E→A(20), K(24)	—[b], 1.9
I→A(20)	—[b]	R→A(20)	0.3
P→A(20)	0.3	I	
S→A(20)	0.4	E→K(24)	2.4
Q→A(20)	0.3	A	
A		^{70}N	
F→A(20)	—[b]	A	
R→A(20)	0.3	F	
G→A(20)	0.4	D	
^{50}L→A(20)	0.3	N	
N→A(20)	0.3	L	
E→A(20)	0.4	L	
		N→Q(26,27)	1.1, 0.7

LRR3	(K_d^r)	LRR4	(K_d^r)
L		L→A(28)	—[b]
S		K→A(28), D(18)	0.4, —[b]
^{80}E→K(25)	—[b]	Y→A(28)	0.1
I(L)→A(20)	0.3	L→A(20,28), I, V, F(28)	—[b], 0.1, 0.4, 0.2
L		S→A(28)	0.2
I→A(20)	—[b]	I→A(20,28), L, V, F(27)	0, 0.2, 0.2, 0.6
Q		C→A(28), S(29), R(30)	0.3, 1.3, —[b]
N		^{110}N→A(28)	0.6
T		T→A(28)	0.6
K		G→A(28)	0.3
N		I→A(28)	0.5
L		R→A(28), E(24)	0.2, 2.1
^{90}R(L)		K(T)→A(28)	0.3
Y		F(L)	
I		P	
E		D→K(18)	—[b]
P		V	
G		^{120}T	
A		K→D(24)	3.4
F		V(I)	
I(T)		F(S)	
N		S	
^{100}L		S	
P		E	
R→A(28)	0.4	S(F)	

LRR5	(K_d^r)	LRR6	(K_d^r)
N		S→A(26,27)	0.5, 0.6
F		V	
^{130}I		T	
L→A(20)	0.4	L→A(20)	0.4
E→K(18)	—[b]	K→R,G,Q,E(25)	1.0, 0.7, 1.0
I→A(20)	0.5	L→A(X)	0.4
C→S(29)	1.4	^{160}Y	
D→K(18)	—[b]	G	
N		N	
L		G	
H		F	
I		E	
^{140}T		E	
T		V	
I		Q	
P		S	
G		^{170}H	
N		A	
A		F	
F		N→Q(26,27)	—[b]
Q		G	
^{150}M		T→A(26,27)	0.4, —[b]
N		T	
N→Q(26,27)	0.3, —[b]		
E			

LRR7	(K_d^r)	LRR8	(K_d^r)
L		P	
T(I)		K(S)	
S		T(I)	
^{180} L→A(20)	0.3	L→A(20)	—[b]
E→K(25)	—[b]	D→E,Q,K(24)	0.2, 0.5, —[b]
L→A(20)	—[b]	I→A(20)	0.3
K→R,G,Q, E(25)	0.2, 0.1, 0.5, —[b]	S	
E→N,K(25)	0.5, —[b]	S	
N		^{210}T	
V(I)		K	
H(Y)		L	
L		Q	
E→K(25)	0.7	A	
^{190}K→E(25)	0.7	L	
M		P	
H		S	
N(S)		Y(H)	
G		G	
A		^{220}L	
F		E→K(24)	0.9
R(Q)		S	
G		I	
A		Q	
^{200}T		R(T)	
G			

[a] The amino acid sequences of the purported eight LRRS of the human LHR ectodomain *(19)* are given; differences between the human and rat sequences are presented as human (rat). The choice of the eight LRRs shown for human LHR *(19)* is essentially identical to that made for the nine LRRs of rat LHR *(17)*; the only difference is that the ninth LRR suggested for rat LHR was not considered since it had an LIA motif instead of (L/I)-X-(L/I). Single replacements via site-directed mutagenesis are indicated, along with the corresponding relative K_d presented as a ratio, $K_d^r = K_d^{wt}/K_d^{mut}$. This ratio ($K_d^r$) is 1.0 if the WT and mutant LHRs have the same affinity, <1.0 if the mutant exhibits reduced affinity compared to WT, and >1.0 if the mutant has greater affinity for ligand than WT receptor.

[b] The specific binding was too low to permit a measurement of the K_d. In many cases, expression of receptor mutant was documented by Western analysis and/or epitope-tagged LHR.

Major portions of LRRs 1, 2, and 4 have been screened, in large part, through the comprehensive investigations by Song et al. *(19,27)*. A number of replacements essentially eliminate ligand binding, even in cases of documented receptor expression (e.g., L32A, I42A, F47A, I56A, I58A, S63A, L64A, E65A, I83A, D118K, E132K, D135K, E184K, and D206K) *(17,19,24)*. While the replacing side chains may drastically alter the conformation of the ectodomain, thus abolishing ligand binding, it is tempting to consider that the WT structures represent important contact sites for receptor-ligand interaction. Most of the replacements of hydrophobic and hydrophilic amino acid residues in the ectodomain reduce ligand binding but do not eliminate it; a few replacements result in enhanced binding. Aside from the caveat of ectodomain conformational change, these results suggest a large number of weak interactions between hCG and LHR, involving nonpolar and polar, ionizable and nonionizable side chains. Bhowmick et al. *(17)* showed that the inner cusp of the putative LHR cusp structure (Fig. 1) has a net negative electrostatic potential surface (Fig. 2), perhaps serving to direct the proper orientation for binding of hCG and providing a favorable surface for charge-charge interactions with a cationic portion of the hormone. As with most protein-protein interactions, it is expected that hydrophobic interactions will be a major contributing factor to the hCG-LHR contact surface. Consistent with this suggestion is the finding of numerous residues in the putative β-strands that appear to be involved in hCG binding *(17,19,24,27)*.

It must be emphasized that the suggested structure depicted in Fig. 1 is only a working model and that unequivocal determination of the ectodomain structure must await detailed crystallographic or nuclear magnetic resonance spectroscopic investigations. The available mutagenesis data, when inter-preted in terms of an LRR structure as shown, suggest that both the β-strands and α-helices, as well as the adjoining loops, are important determinants for ligand binding *(17–19,24,27)*. Proposals exist for docking hCG to the LHR ectodomain *(14,16)*, but, again, definitive information must await a structure for the receptor.

Spectroscopic Study of LHR Ectodomain

Aside from the mutagenesis studies already reviewed, there is very little experimental evidence directed toward elucidating the conformation of the ectodomains. A report recently appeared on the circular dichroic spectrum of a complex of hCG and the LHR ectodomain *(30)*. The spectrum was characterized by a minimum and a maximum at 210 and 191 nm, respectively. Spectral deconvolution yielded about 17% α-helix and 30–35% β-sheets; correcting for the expected contribution of hCG, it was estimated that the ectodomain may be 25–30% α-helix and 30–35% β-sheets. These numbers are in reasonable agreement with those obtained by circular dichroic analysis of the ectodomain of the homologous protein hFSHR *(31,32)*. For the latter, minima were observed at about 207–208 and 221 nm and a maximum at 190 nm, and α-helical and β-sheet contents were estimated to be about 23% each, with some 21% β-turns. Interestingly, a single chain complex of FSH bound to the FSHR ectodomain yielded secondary structure estimates of 7% α-helix, 35% β-sheets, and 19% β-turns, and there was evidence of a conformational shift concomitant with ligand binding.

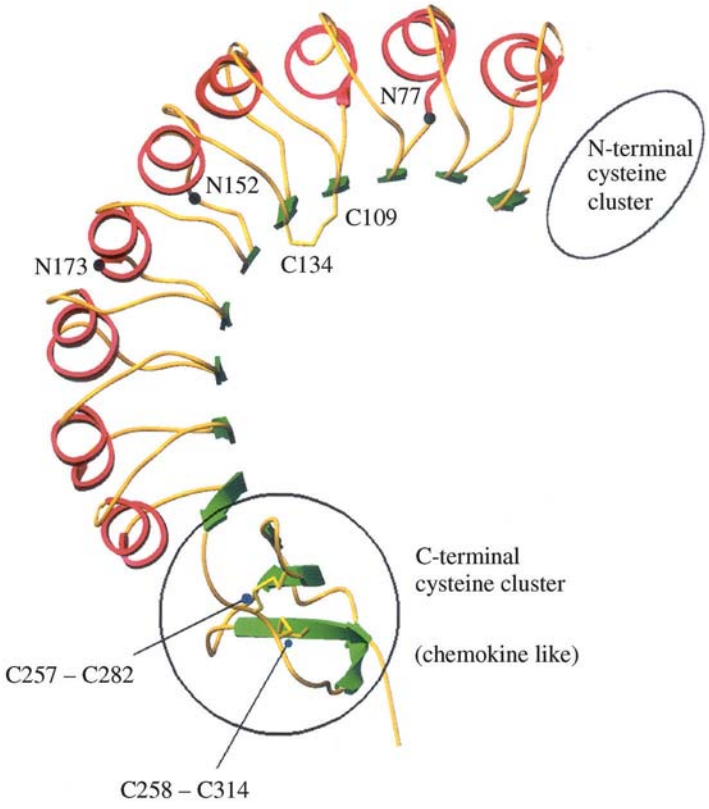

Fig. 1. Molecular model of ectodomain (amino acid residues 27–235) of WT LHR based on nine LRRs. The N-terminal cysteine-rich region has not been modeled, and the C-terminal cysteine-rich region is schematically shown in a chemokine-like fold. (From ref. *17* with permission of the Endocrine Society.)

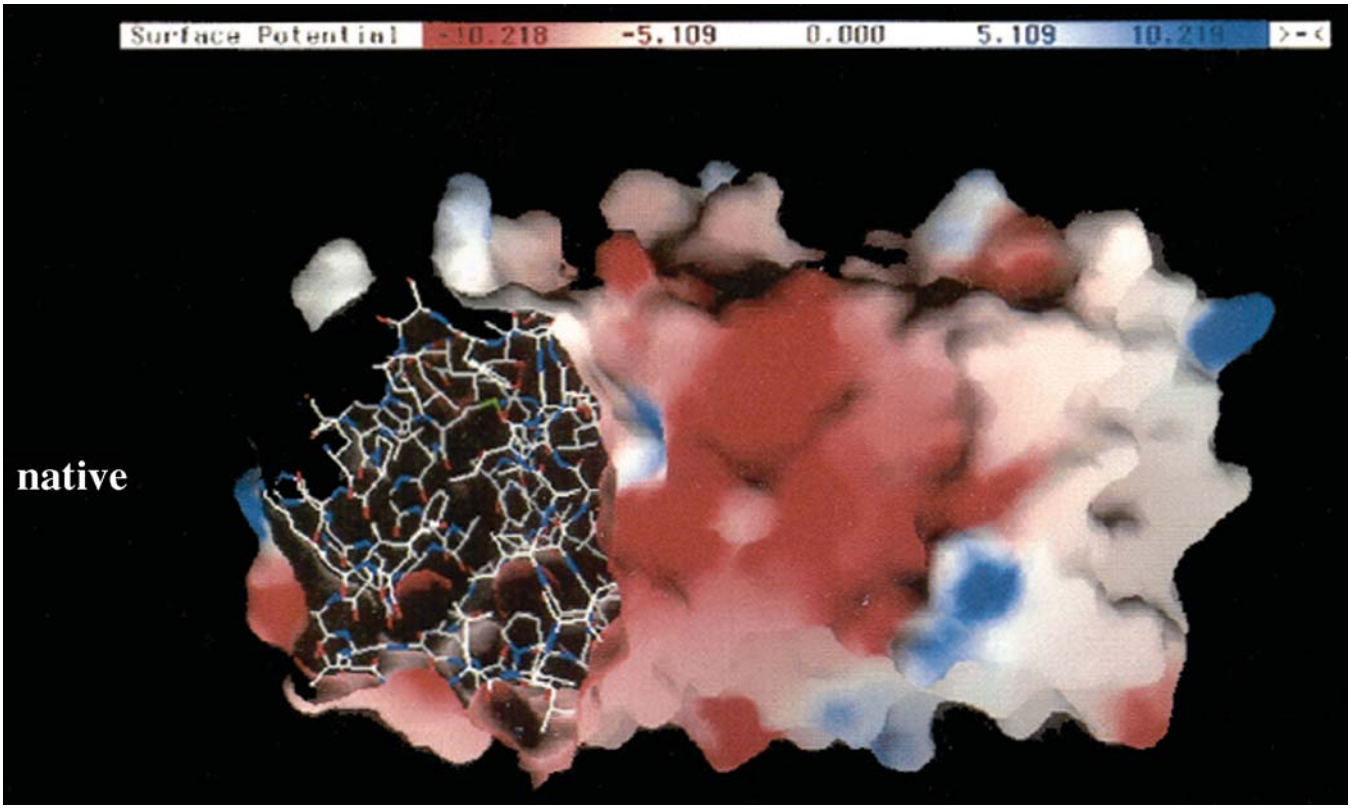

Fig. 2. Electrostatic potential surface of inner cusp of WT (native) LHR model depicted in Fig. 1. The region is negatively charged and may influence ligand binding. (From ref. *18* with permission of the Endocrine Society.)

These secondary structure estimates of the ecotodomains of human LHR *(30)* and FSHR *(31,32)* are reasonably consistent with values expected from an LRR protein such as ribonuclease inhibitor *(20)*. It must be emphasized, however, that the experimental data on site-directed mutagenesis and circular dichroic spectroscopy do not, in and of themselves, confirm the purported LRR-like structure. Moreover, there are major parts of the ectodomain, such as those encoded by most of exon 1 (i.e., the N-terminus), much of exon 9, exon 10, and a portion of exon 11 (i.e., the large Cys-rich cluster prior to transmembrane helix 1), for which there are no structural working models; these regions are also believed to be important in ligand binding and receptor activation.

Ab Initio Modeling of Endodomain

The first molecular model of the LHR built by one of us (F.F.) followed an ab initio procedure based on the integration of computational chemistry and bioinformatics tools with the results of mutational, biophysical, and biochemical experiments on GPCRs *(11)*. The ab initio LHR model also holds the structural information as inferred from the electron micrographs of three-dimensional frog rhodopsin crystals *(33)*, as well as from the analysis of ~500 GPCR sequences *(34)*, and comprises the seven transmembrane helices and the connecting extracellular and intracellular loops. Comparative molecular dynamics (MD) simulations, by means of the program CHARMm *(35)*, have been performed on WT LHR, as well as on all the naturally occurring activating and inactivating mutations discovered thus far *(2,4,5,36)*. The strategy used has been to elaborate a unique input structure, such as one that is the same for the WT and the mutants except for the mutated amino acid side chain, and to produce, on MD simulations, divergent average arrangements for the active and inactive receptor forms *(11)*.

The average minimized structure of the WT LHR achieved by ab initio modeling shows a root mean square deviation (RMSD) of 4.57 Å from the rhodopsin structure *(9)*. The RMSD was computed by superimposing the main-chain atoms of segments 37–62, 74–99, 111–133, 152–171, 202–225, 253–276, and 286–306, representing the seven transmembrane domains of rhodopsin, with those in the homologous segments 359–384, 396–422, 440–462, 482–501, 526–549, 570–593, and 603–623 of the average minimized structure of the WT LHR. Note that, according to the same fitting criteria, the transmembrane seven-helix bundle of the LHR input shows an RMSD of 6.00 Å from the rhodopsin structure. This suggests that the computation conditions allow for a convergence between the LHR model and the rhodopsin structure.

In general, the length of the seven helices in the ab initio LHR model is in good agreement with that found in the rhodopsin structure. The largest deviations between the WT LHR model and the rhodopsin structure are mainly owing to the arrangements of helices 2 and 3. Helix 2 in rhodopsin starts three amino acids earlier compared to the LHR model. Moreover, in the rhodopsin structure, helix 3 has a more tilted orientation so that its cytosolic end is closer to helix 5 than in the LHR model. As a consequence of these differences, the conserved aspartate in helix 2 (D83) and the arginine of the E/D-R-Y/W sequence (R135) in rhodopsin are too far apart for interacting, and the ground state of the photoreceptor is characterized by a salt bridge interaction between this arginine and both E134 and E247. Moreover, the cytosolic extensions of helices 5 and 6 are rotated in a slightly different way in the LHR model compared to the rhodopsin structure. Other differences are that the amino acid segment F293-V300 in rhodopsin shows a non-α-helix conformation and that the K311-C322 segment at the C-terminus of helix 7 is tilted at a sharper angle.

Structural Features of Mutation-Induced Active and Inactive LHR States Within Ab Initio Models

The structural features characterizing the mutation-induced inactive and active states of the LHR have been inferred by comparing the average minimized structures of WT LHR to all the naturally occurring active and inactive mutants known thus far *(4,5,36)*. According to the results of MD analysis, constitutively active LHR mutants share the release of the constraining salt bridge interactions found in WT LHR and its inactive mutants between R464 of the E/D-R-Y/W motif in the cytosolic extension of helix 3 and the conserved D405 in helix 2 and/or the adjacent E463 in helix 3. Another feature shared by the LHR constitutively active mutants is the opening of a crevice between the second and third intracellular loops (i2 and i3, respectively) which might contribute to the receptor–G protein interface.

These results are consistent with the experimental findings that the sequences connecting helices 3 to 4 and 5 to 6 in rhodopsin are involved in binding and/or activation of transducin (G_t), whereas the peptide corresponding to the 1–2 interhelical sequence of rhodopsin does not compete with metarhodopsin II for binding to G_t *(37,38)*. The important role of i2 and i3 in G protein recognition is also consistent with several experimental findings on other GPCRs *(39–41)*. The opening of a crevice between i2 and i3 allows solvent exposure of the intracellular extensions of helices 3 and 6. In particular, the 563–574 stretch of amino acids lying in the cytosolic extension of helix 6 becomes exposed to the solvent in the constitutively activating mutants and might play a role in receptor–G protein recognition. These results are consistent with the experimental findings that a peptide from the sequence 570–577 of LHR is capable of activating G_s *(42)*.

Two theoretical indices properly account for the structural differences between the active and inactive LHR forms, thus providing a useful tool for computer simulation–based predictions of the functional behavior of new LHR mutants (Fig. 3). These theoretical descriptors are (1) the distance between the γ-carbon atom of D405 and the ζ-carbon atom of R464, and (2) the solvent-accessible surface of W465 (SAS_{W465}).

Differently from WT LHR and the inactive mutants, constitutively active mutants have been found to have both D405-R464 distances >4.7 Å and SAS_{W465} values >32.0 $Å^2$. Values of SAS_{W465} >32.0 $Å^2$ correlate with the opening of the cytosolic crevice between i2 and i3. These indexes have also been used to investigate the LHR sites potentially susceptible to activating mutations *(11)*.

Comparative Modeling of Endodomain

Very recently, a new model of the human LHR has been achieved by comparative modeling *(5,13)* using the MODELLER program *(43)* and the crystal structure of rhodopsin as a template *(9)*. The WT and mutant structures were energy minimized and subjected to MD simulations following the same computational protocol as that previously used for the ab initio models *(11)*. The receptor structures, averaged over the 200 structures collected during the last 100 ps of a 150-ps MD trajectory and minimized, were then employed for the comparative analysis.

The LHR input structure shows an RMSD of 0.24 Å from the rhodopsin structure (RMSD has been computed considering the matching criteria described earlier for the ab initio model). This deviation increases on average by 2 Å following energy minimizations and MD simulations. In fact, the average minimized structures of WT LHR diverges from the rhodopsin structure by 2.54 Å. These deviations are close to the expected values, considering the sequence identity (22.2%) between the matched segments of the LHR and rhodopsin *(44)*.

Structural Features of Mutation-Induced Active and Inactive LHR States Within Homology Models

As with the ab initio model, one of the structural modifications that occurs with constitutive activation is a change in the interaction patterns involving R464, the highly conserved residue of the E/D-R-Y/W motif (highlighted in purple in Fig. 4). In fact, according to the rhodopsin-based model, R464 in the inactive structure is predicted to participate in a double salt bridge with both the adjacent E463 and D564 in the cytosolic extension of helix 6, a residue that results in constitutive activation when mutated *(45,46)*. A similar interaction pattern is found in the high-resolution crystal structure of rhodopsin *(9)* between R135 (homologous to R464 in LHR) and both the adjacent E134 and E247 (homologous to E463 and D564, respectively, in LHR). In the constitutively active LHR mutants, R464 is predicted to lose its interactions with one or both of these anionic amino acids, thus becoming more exposed to the solvent. Whether the fully conserved arginine is essential for LHR activation or G protein recognition/activation still remains unclear.

Thus, the homology model suggests that the R464-D564 salt bridge contributes to the stabilization of the inactive state of the LHR linking the cytosolic extensions of helices 3 and 6. The destabilization or breakage of the interaction involving R464 in the inactive state of LHR is predicted to result in an increase in the solvent accessibility of the cytosolic extensions of helices 3 and 6. This structural effect is properly described by the solvent-accessible surface area computed over selected amino acids. In fact, this index is a good hallmark of the functional receptor state, being below 50 $Å^2$ in the inactive LHR forms and above that threshold in the active ones *(5,13)*, and it has proven effective in predicting the outcome of combining functionally similar or different mutants *(13)*.

Structural Features of Activating Mutation Sites

Despite the differences between them, both the ab initio and homology models suggest that the sites susceptible to activating mutations are interhelical positions close to highly conserved polar amino acid residues (i.e., N377, D405, S453, R464, N615, S616, N619, and Y623) that are mainly located in the cytosolic halves of helices 1–3 and 7 (Fig. 4) *(11)*. Four of these eight conserved polar amino acids are found in helix 7 and include two members of the conserved NPXXY motif (i.e., N619 and Y623).

Both the ab initio and homology models suggest that activating mutations may cause either gain or loss, or just change the interaction of the native amino acid. In some receptor sites, only selected substitutions cause constitutive activity. This is the case of L457, for which experimental findings suggest that only replacement with cationic amino acids leads to constitutively active forms of the LHR *(12)*. Computer simulations on both the ab initio and homology models suggest that the need for a cationic amino acid in position 457 triggering constitutive activation is linked to the closeness of D578 in helix 6, which would stabilize the active state of the receptor by forming a salt bridge with the cationic amino acid side chain substituting for L457 *(11,12)*. Furthermore, for some receptor sites, the extent of constitutive activity is independent of the amino acid substitution. This is the case of D564 and D578. For D564, experiments have shown that substitution of this aspartate with G, A, V, L, F, K, and N, which would break or weaken a salt bridge with a putative cationic amino acid, results in constitutive activation, whereas substitution with glutamate does not *(45,46)*. Consistent with these experimental findings, simulations on the ab initio and homology models suggest that the stabilizing effect of D564 on the inactive state of the LHR is exerted via an interhelical salt bridge rather than via an intrahelix H-bonding interaction, as recently suggested *(47)*.

For D578, experiments have shown that replacement of D578 with nine different natural amino acids induces constitutive activation of LHR, independently of the physicochemical properties of the substituting amino acid, the mutation to asparagine showing a normal activity *(48)*. Both of the theoretical models suggest that the activating mutations of D578 cause the breakage or simply a perturbation in the H-bonding interaction involving D578 in the WT LHR. In particular, simulations on the homology model suggest that in the WT LHR, D578 is involved in H-bonding interactions with the

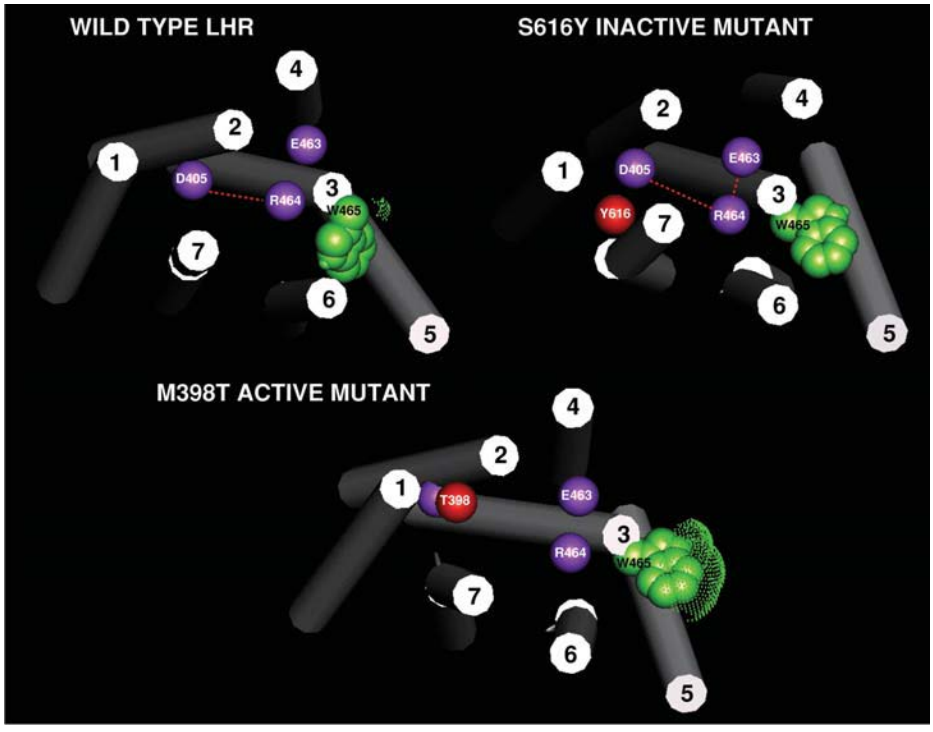

Fig. 3. Average minimized structures of endodomain (transmembrane helices) of WT LHR (**top left**), S616Y inactive mutant (**top right**), and M398T constitutively active mutant (**bottom**). The helix bundles are represented by cylinders and are viewed from the intracellular side in a direction almost perpendicular to the membrane surface. The highly conserved D405, E463, and R464 are represented by a sphere centered on the β-carbon atom of the amino acid side chain. The mutated positions are indicated by red spheres centered on the β-carbon atom of the side chain. The W465 side chain is represented by van der Waals spheres. Dashed red lines indicate intramolecular interactions. Green dots represent the solvent-accessible surfaces computed on the W465 side chain.

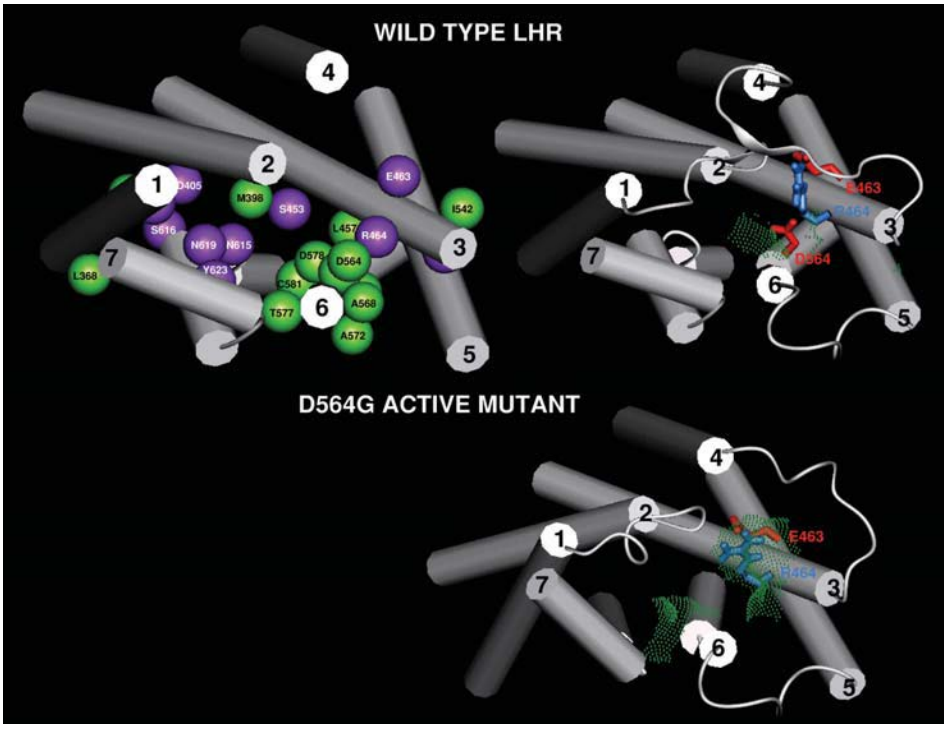

Fig. 4. Average minimized structures of endodomain (transmembrane helices) of WT LHR (**top**) and D564G constitutively active mutant (**bottom**). The helix bundles are represented by cylinders and are viewed from the intracellular side in a direction almost perpendicular to the membrane surface. In one view of the WT LHR (**top left**), the receptor sites susceptible to spontaneous activating mutations are represented by green spheres, whereas the positions of the highly conserved amino acids are represented by purple spheres. In the top right view of the WT and in the D564G mutant (bottom), the side chains of E463, R464, and D564 are represented by sticks. The composite solvent-accessible surface computed over the amino acids R464, T467, I468, and K563 is also shown, represented by green dots.

highly conserved N615 in helix 7 *(13)*. Computer-simulated and experimental mutagenesis also suggest that the integrity of the highly conserved N615 and N619 in helix 7 is essential for the constitutive activity of the D578 mutants *(13)*.

In some other cases, it is possible to find quantitative relationships between the physicochemical properties of the replacing amino acid and the extent of the constitutive activity induced by the mutation. This is the case of M398, which has been subjected to 15 different amino acid substitutions (F. Fanelli, M. Verhoef-Port, M., Timmerman, A. Zeilemaker, J. W. M. Martens, and A. P. N. Themmen, unpublished observations). Indeed, the basal activity of the M398 mutants is inversely correlated with the size of the replacing amino acid. Consistent with this relationship, molecular simulations have suggested that reducing the size of the amino acid at position 398 reduces the intramolecular interactions of the mutated amino acid and confers to the receptor structure the features of the active form(s). It has been suggested that the highly conserved Y621 of the NPXXY motif in helix 7 mediates this effect.

In summary, both the ab initio and the rhodopsin-based models of the endodomain converge into the hypothesis that, despite the topological and structural differences between them, the activating mutation sites are structurally connected to peculiar portions of the cytosolic domains. In fact, activating mutations weaken the ground state interactions of R464 and increase the solvent accessibility of selected amino acids at the cytosolic extensions of helices 3 and 6. This structural effect would be mediated by highly conserved polar amino acids in the seven-helix bundle.

Conclusion

The results of molecular simulations on different LHR models suggest that a structural modification at the interface between the cytosolic extensions of helices 3 and 6 is important in the mutation-induced LHR activation and/or G protein recognition. This hypothesis is consistent with a number of studies demonstrating that a rearrangement in the relative position of helices 3 and 6 is a fundamental step in GPCR activation *(3,49,50)*. The next challenge in our study will consist of building a more complex LHR model including both the ecto- and endodomains in order to gain insight into the structural modifications induced by hormone binding.

Acknowledgments

It is a pleasure to thank Dr. Prema Narayan for her interest in this research and for critically reviewing the manuscript. This work was supported by CNR and CICAIA, University of Modena and Reggio Emilia and Telethon-Italy (grant no. 68/cp), and grant NIH-DK33973. F. F. is an Assistant Telethon Scientist (DTI, Fondazíone Telethon).

References

1. Simoni, M., Gromoll, J., and Nieschlag, E. (1997). *Endocr. Rev.* **18,** 739–773.
2. Dufau, M. (1998). *Annu. Rev. Physiol.* **60,** 461–496.
3. Gether, U. (2000). *Endocr. Rev.* **21,** 90–113.
4. Fanelli, F., Themmen, A. P. N., and Puett, D. (2001). *IUBMB Life* **51,** 149–155.
5. Ascoli, M., Fanelli, F., and Segaloff, D. L. (2002). *Endocr. Rev.* **23,** 141–174.
6. Hearn, M. T. W. and Gomme, P. T. (2000). *J. Mol. Recogn.* **13,** 223–278.
7. Koo, Y. B., Ji, I., Slaughter, R. G., and Ji, T. H. (1991). *Endocrinology* **128,** 2297–2308.
8. Tsai-Morris, C. H., Buczko, E., Wang, W., Xie, X.-Z., and Dufau, M. L. (1991). *J. Biol. Chem.* **266,** 11,355–11,359.
9. Palczewski, K., Kumasaka, T., Hori, T., Behnke, C. A., Motoshima, H., Fox, B. A., Le Trong, I., Teller, D. C., Okada, T., Stenkamp, R. E., Yamamoto, M., and Miyano, M. (2000). *Science* **289,** 739–745.
10. Lin, Z., Shenker, A., and Pearlstein, R. (1997). *Prot. Engr.* **10,** 501–510.
11. Fanelli, F. (2000). *J. Mol. Biol.* **296,** 1333–1351.
12. Shinozaki, H., Fanelli, F., Liu, X., Nakamura, K., and Segaloff, D. L. (2001). *Mol. Endocrinol.* **15,** 972–984.
13. Angelova, K., Fanelli, F., and Puett, D. (2002). *J. Biol. Chem.* **277,** 32202–32213.
14. Moyle, W. R., Campbell, R. K., Rao, S. N. V., Ayad, N. G., Bernard, M. P., Han, Y., and Wang, Y. (1995). *J. Biol. Chem.* **270,** 20,020–20,031.
15. Kajava, A. V., Vassart, G., and Wodak, S. (1995). *Structure* **3,** 867–877.
16. Jiang, X., Dreano, M., Buckler, D. R., Cheng, S., Ythier, A., Wu, H., Hendrickson, W. A., and Tayar, N. E. (1995). *Structure* **3,** 1341–1353.
17. Bhowmick, N., Huang, J., Puett, D., Isaacs, N. W., and Lapthorn, A. J. (1996). *Mol. Endocrinol.* **10,** 1147–1159.
18. Couture, L., Naharisoa, H., Grebert, D., Remy, J.-J., Pajot-Augy, E., Bozon, V., Haertle, T., and Salesse, R. (1996). *J. Mol. Endocrinol.* **16,** 15–25.
19. Song, Y. S., Ji, I., Beauchamp, J., Isaacs, N. W., and Ji, T. H. (2001). *J. Biol. Chem.* **276,** 3426–3435.
20. Kobe, B. and Deisenhofer, J. (1993). *Nature* **366,** 751–756.
21. McFarland, K. C., Sprengel, R., Phillips, H. S., Kohler, M., Rosemblit, N., Nickolics, K., Segaloff, D. L., and Seeburg, P. H. (1989). *Science* **245,** 494–499.
22. Loosfelt, H., Misrahi, M., Atger, M., Salesse, R., Vu Hai-Luu Thi, M. T., Jolivet, A., Guiochon-Mantel, A., Sar, S., Jallal, B., Garnier, J., and Milgrom, E. (1989). *Science* **245,** 525–528.
23. Huang, J. and Puett, D. (1995). *J. Biol. Chem.* **270,** 30,023–30,028.
24. Bhowmick, N., Narayan, P., and Puett, D. (1999). *Endocrinology* **140,** 4558–4563.
25. Liu, X., Davis, D., and Segaloff, D. L. (1993). *J. Biol. Chem.* **268,** 1513–1516.
26. Zhang, R., Cai, H., Fatima, N., Buczko, E., and Dufau, M. L. (1995). *J. Biol. Chem.* **270,** 21,722–21,728.
27. Song, Y. S., Ji, I., Beauchamp, J., Isaacs, N. W., and Ji, T. H. (2001). *J. Biol. Chem.* **276,** 3436–3442.
28. Zhang, R., Buczko, E., and Dufau, M. L. (1996). *J. Biol. Chem.* **271,** 5755–5760.
29. Misrahi, M., Meduri, G., Pissard, S., Bouvattier, C., Beau, I., Loosfelt, H., Jolivet, A., Rappoport, R., Milgrom, E., and Bougneres, P. (1997). *J. Clin. Endocrinol. Metab.* **82,** 2159–2165.
30. Remy, J.-J., Nespoulous, C., Grosclaude, J., Grebert, D., Couture, L., Pajot, E., and Salesse, R. (2001). *J. Biol. Chem.* **276,** 1681–1687.
31. Mahale, S. D., Cavanagh, J., Schmidt, A., MacColl, R., and Dias, J. A. (2001). *J. Biol. Chem.* **276,** 12,410–12,419.

32. Schmidt, A., MacColl, R., Lindau-Shepard, B., Buckler, D. R., and Dias, J. A. (2001). *J. Biol. Chem.* **276,** 23,373–23,381.
33. Unger, V. M., Hargrave, P. A., Baldwin, J. M., and Schertler, G. F. X. (1997). *Nature* **389,** 203–206.
34. Baldwin, J. M., Schertler, G. F., and Unger, V. M. (1997). *J. Mol. Biol.* **272,** 144–164.
35. Brooks, B. R., Bruccoleri, R. E., Olafson, B. D., States, D. J., Swaminathan, S., and Karplus, M. (1983). *J. Comput. Chem.* **4,** 187–217.
36. Themmen, A. P. N. and Huhtaniemi, I. T. (2000). *Endocr. Rev.* **21,** 551–583.
37. Franke, R. R., Sakmar, T., Graham, R. M., and Khorana, H. G. (1992). *J. Biol. Chem.* **267,** 14,767–14,774.
38. Klein-Seetharaman, J., Hwa, J., Cai, K., Altenbach, C., Hubbell, W. L., and Khorana, H. G. (1999). *Biochemistry* **38,** 7938–7944.
39. Wess, J. (1997). *FASEB J.* **11,** 346–354.
40. Burstein, E. S., Spalding, T. A., and Brann, M. R. (1998). *J. Biol. Chem.* **273,** 24,322–24,327.
41. Burstein, E. S., Spalding, T. A., and Brann, M. R. (1998). *Biochemistry* **37,** 4052–4058.
42. Abell, A. N. and Segaloff, D. L. (1997). *J. Biol. Chem.* **272,** 14,586–14,591.
43. Sali, A. and Blundell, T. L. (1993). *J. Mol. Biol.* **234,** 779–815.
44. Chothia, C. and Lesk, A. M. (1986). *EMBO J.* **5,** 823–826.
45. Schulz, A., Schöneberg, T., Paschke, R., Schultz, G., and Gudermann, T. (1999). *Mol. Endocrinol.* **13,** 181–190.
46. Schoneberg, T., Schultz, G., and Gudermann, T. (1999). *Mol. Cell. Endocrinol.* **151,** 181–193.
47. Kudo, M., Osuga, Y., Kobilka, B. K., and Hsueh, A. J. W. (1996). *J. Biol. Chem.* **271,** 22,470–22,478.
48. Kosugi, S., Mori, T., and Shenker, A. (1996). *J. Biol. Chem.* **271,** 31,813–31,817.
49. Sheikh, S. P., Zvyaga, T. A., Lichtarge, O., Sakmar, T. P., and Bourne, H. R. (1996). *Nature* **383,** 347–350.
50. Farrens, D. L., Altenbach, C., Yang, K., Hubbell, W. L., and Khorana, H. G. (1996). *Science* **274,** 768–770.